Nuclear Physics A514 (1990) 49-65
North-Holland

GAMOW-TELLER STRENGTH OBSERVED IN THE ^{48}Ti(n, p)^{48}Sc REACTION: Implications for the double beta decay of ^{48}Ca

W.P. ALFORD and R.L. HELMER[1]
University of Western Ontario, London, Ont., Canada N6A 3K7

R. ABEGG, A. CELLER, D. FREKERS, P. GREEN, O. HÄUSSER, R. HENDERSON, K. HICKS[2], K.P. JACKSON, R. JEPPESEN[3], C.A. MILLER, A. TRUDEL, M. VETTERLI and S. YEN
Triumf, Vancouver, B.C., Canada V6T 2A3

R. POURANG and J. WATSON
Kent State University, Kent, OH 44242, USA

B.A. BROWN
National Superconducting Cyclotron Laboratory
and
Department of Physics and Astronomy, Michigan State University, East Lansing, MI 48824, USA

J. ENGEL[4]
California Institute of Technology, Pasadena, CA 91125, USA

Received 23 November 1989
(Revised 27 February 1990)

Abstract: Cross sections for the ^{48}Ti(n, p) reaction have been measured at angles of 0°, 6°, and 12° at an energy of 200 MeV. The measurements are compared with results of DWIA calculations to obtain estimates of transition strengths for $L = 0$, 1, and ≥ 2 up to an excitation energy of 25 MeV. Gamow-Teller strength ($L = 0$) is peaked between 3 and 4 MeV excitation energy, with a significant distribution extending to about 12 MeV. The $L = 1$ strength is found mainly between 6 and 20 MeV while the cross section for transitions with $L \geq 2$ increases from 10 MeV to the upper limit of the measurements. The distribution of Gamow-Teller strength is in poor agreement with theoretical distributions used to calculate the lifetime for double beta decay of ^{48}Ca.

E | NUCLEAR REACTIONS: ^{48}Ti(n, p), $E = 198$ MeV; measured $\sigma(\theta)$. ^{48}Sc deduced Gamow-Teller strength distribution. Shell model comparison.

[1] Present address: TRIUMF, Vancouver, B.C., Canada V6T 2A3.
[2] Present address: Ohio University, Athens, OH 45701-2979, USA.
[3] Present address: Los Alamos National Laboratory, Los Alamos, NM 87545, USA.
[4] Present address: Bartol Research Institute, University of Delaware, Newark DL 19716, USA.

1. Introduction

Studies of the (p, n) reaction at intermediate energies ($E_p > 100$ MeV) have shown that the reaction cross section is determined mainly by the isovector spin-transfer component of the effective interaction [1]). For small momentum transfer, i.e. at forward angles and low excitation energy, transitions with $L = 0$ are dominant, so that under these experimental conditions, the (p, n) reaction should excite transitions analogous to allowed Gamow-Teller β^- decay between the same states. In fact, it has been shown that the forward-angle (p, n) cross section, extrapolated to zero momentum transfer, is proportional to the strength of the allowed GT beta transition between the same states [2]). More extensive studies have demonstrated significant deviations from strict proportionality [3]) but (p, n) cross-section measurements still provide useful estimates of GT transition strength, especially for transitions energetically forbidden in beta decay. A similar proportionality has been demonstrated between (n, p) cross sections at zero momentum transfer and Gamow-Teller transition strengths for β^+ decay [4]). These correspondences have been used to investigate the problem of missing strength in the GT sum rule [5-7]), to calibrate proposed detectors for solar neutrinos [8]), and to study strength distributions of interest for electron capture processes, which may be important in late stages of stellar evolution [7]). It has also been pointed out that they may provide useful information relating to the process of double beta decay [9]).

Double beta decay with emission of two neutrinos occurs as a second-order weak transition, which has been extensively studied and has been observed or inferred in a few cases [10,11]). Neutrinoless double beta decay is a lepton-number-violating process, which is forbidden in the standard electroweak theory, but which is predicted to occur if the neutrino is a Majorana particle with non-zero mass [12]). A number of careful searches have failed to observe neutrinoless decay, but lifetime limits have been established which have been interpreted in terms of limits on neutrino mass [13]).

For the allowed second-order decay with emission of two neutrinos, the decay amplitude involves the quantity [14]):

$$M_{2\nu} = \sum_{\mathrm{m}} \frac{\langle \mathrm{f} \| t_- \boldsymbol{\sigma} \| \mathrm{m} \rangle \langle \mathrm{m} \| t_- \boldsymbol{\sigma} \| \mathrm{i} \rangle}{E_{\mathrm{xm}} + \Delta M + \frac{1}{2} T_0} . \tag{1}$$

where $T_0 = 4.271$ MeV is the energy released in the decay, $\Delta M = -0.281$ MeV is the atomic mass difference between ^{48}Sc and ^{48}Ca and E_{xm} are excitation energies of intermediate states $|\mathrm{m}\rangle$ with $J^\pi = 1^+$. The decay rate is then given by

$$\lambda_{2\nu} = f_{2\nu} |M_{2\nu}|^2 ,$$

where $f_{2\nu}$ is a phase space factor for emission of two electrons plus two neutrinos with the total decay energy shared among the four particles. The estimation of decay rates then involves a nuclear structure calculation for matrix elements of the allowed Gamow-Teller transition operator for 1^+ states in the intermediate nucleus.

For neutrinoless decay arising from the existence of a Majorana neutrino of mass m_ν the transition probability may be written

$$\lambda_{0\nu} = f_{0\nu} |M_{0\nu}|^2 m_\nu^2 . \tag{2}$$

In this expression $f_{0\nu}$ is the phase space factor for emission of two electrons only which carry the total energy released in the decay, $M_{0\nu}$ the nuclear matrix element for 0ν decay and m_ν the finite neutrino mass. From measured limits for the 0ν lifetime plus model calculations of $M_{0\nu}$, eq. (2) has been used to set upper limits on the mass of a possible Majorana neutrino [13,15]).

A problem with this approach is suggested by the fact that many of the calculations of 2ν decay lifetimes yield results which are up to two orders of magnitude shorter than observed lifetimes or limits [16]). More recent calculations based on a quasi-particle random-phase approximation (QRPA) have shown that the inclusion of particle-particle interactions can increase the predicted lifetimes dramatically with suitable choice of interaction strength [17,18]). While agreement with experiment can be obtained, the sensitivity to the magnitude of the interaction strength results in large uncertainty in the calculated lifetime for 2ν decay. For 0ν decay, the matrix element is taken between the same initial and final states as in 2ν decay, and thus involves some of the same nuclear structure wave functions required in the calculation of $M_{2\nu}$. However, the nuclear matrix element for neutrinoless decay expressed as a summation over intermediate states involves all multipolarities for the intermediate states in ^{48}Sc, in contrast to the two-neutrino matrix element of eq. (1) which involves only the 1^+ intermediate states. Calculations [12,14,16,19]) show a strong cancellation for the sum over intermediate 1^+ states and hence a great model sensitivity for the two-neutrino decay. The cancellations appear to be not so severe for the other multipoles involved in the neutrinoless decay [19,20]), and hence the model sensitivity is not so great. In any case, knowledge of the Gamow-Teller strength to the 1^+ states provides the crucial ingredient for the two-neutrino decay calculation and an important test of the wave functions for the neutrinoless calculation.

As noted above, it has now been well established that the magnitude of GT matrix elements may be determined from measurements of intermediate energy (p, n) and (n, p) cross sections at small momentum transfer. As a result, the double beta decay matrix elements between initial and intermediate states may be obtained from (p, n) cross-section measurement in the initial nucleus, while those between intermediate and final states are measured by the (n, p) cross sections in the final nucleus.

In practice, with the limited energy resolution available in such measurements, it is not possible to demonstrate that both (p, n) and (n, p) branches proceed through a single intermediate state. It is also not possible to determine the sign of the matrix

element, which is required in the lifetime calculation. Nevertheless, these measurements can provide an estimate of the minimum possible lifetime for a given decay. What is most important is that they measure the distribution of GT strength, which must be reproduced by the structure calculations as a first requirement in calculations of double beta decay lifetimes.

2. Experiment

Measurements were carried out using the TRIUMF charge exchange facility which is shown schematically in fig. 1 for (n, p) measurements. Approximately monoenergetic neutrons are produced in target T, by the ^{7}Li(p, n)^{7}Be reaction. The incident proton beam is then deflected by 20° and directed to a shielded beam dump. Neutrons produced near 0° at T then bombard the target of interest, T_2, and protons from the (n, p) reaction at T_2 are detected in the medium-resolution spectrometer. Target T_2 consists of several layers of the target material mounted between wire chamber planes, which serve to identify the target layer in which each proton originates. A

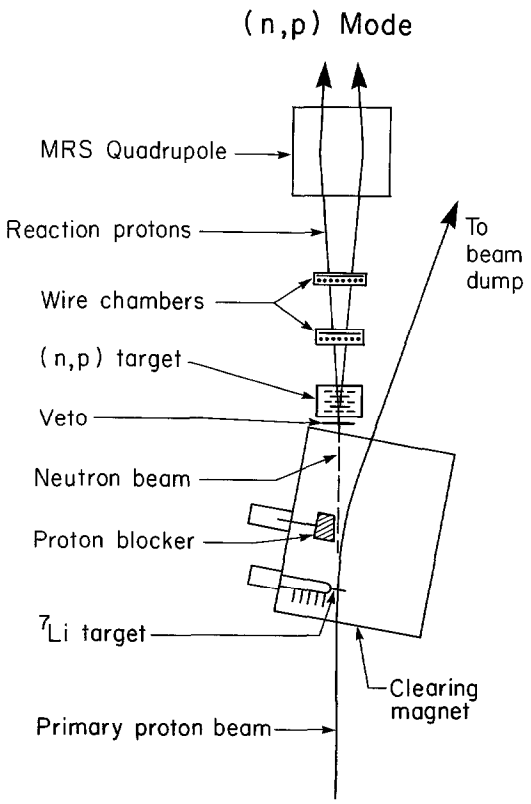

Fig. 1. Layout of the TRIUMF (n, p) facility.

correction for energy loss in subsequent layers is easily made, thus permitting the use of a large total target thickness while maintaining energy resolution comparable to the energy loss in a single target layer. In addition, one of the target layers is usually taken to be polyethylene, so that the neutron flux on the target stack can be determined from the yield of the ^{1}H(n, p) reaction. More complete descriptions of the overall system and of the target box are given elsewhere [21,22]).

Targets used in these measurements were made of material enriched to >99% in ^{48}Ti. One target layer was titanium metal, 130 mg/cm^2 in thickness. Four other targets were fabricated of TiO_2 powder contained between layers of Mylar, 0.8 mg/cm^2 in thickness. The thickness of each target was determined by weighing with an uncertainty of 2%. The polyethylene (CH_2) target used for monitoring neutron flux was initially 187 mg/cm^2 in thickness, but was replaced by a target 11.9 mg/cm^2 in thickness for about half the measurements. The incident proton beam energy was 200 MeV. The neutron production target was of ^{7}Li enriched to >99.9%, 200 mg/cm^2 in thickness. The overall energy resolution of the system, as determined from the line shape observed in the ^{1}H(n, p) reaction, was 1.2 MeV FWHM for the target closest to the entrance to the MRS. Resolution deteriorated to about 1.6 MeV for the target farthest from the MRS because of straggling in intervening targets.

Proton spectra from the ^{48}Ti(n, p)^{48}Sc reaction were measured at angles of 0°, 6° and 12°. Those were the angles for scattering from target centre to the central ray traversing the MRS. Because of the finite size of target T_2 (2×5 cm) and finite acceptance of the MRS, reaction products are observed over a range of scattering angles at each setting of the MRS. The actual distribution of scattering angles was measured during data acquisition and was later used to average the results of DWIA calculations for comparison with experiment.

Proton spectra at 0° from the target of metallic ^{48}Ti, and from the targets of TiO_2, are shown in fig. 2. For excitation energies greater than 6 MeV in ^{48}Sc, the spectrum from the oxide targets is dominated by protons from ^{16}O(n, p) ($Q_0 = -9.64$ MeV) and provides no useful information for the reaction of interest.

These spectra have been corrected for the effect of the neutron spectrum from the ^{7}Li target. The ^{7}Li(p, n) reaction at intermediate energies populates the ground and 0.43 MeV excited states of ^{7}Be with comparable intensities, although these two lines are not resolved in the present measurements. In addition, the spectrum shows a continuum due to many-body final states with an intensity of about 1% per MeV relative to the (g.s. + 0.43 MeV) transitions. Using the measured ^{7}Li(p, n) spectrum shape, the raw spectra were deconvoluted to yield the corrected spectra shown in figs. 2 and 3 for further analysis.

As noted earlier, neutron flux in the measurements was determined from the yield of the ^{1}H(n, p) reaction on a CH_2 target included in the target assembly. For the determination of cross sections, this measured flux required correction for individual titanium targets because of geometrical variation of neutron flux along the target

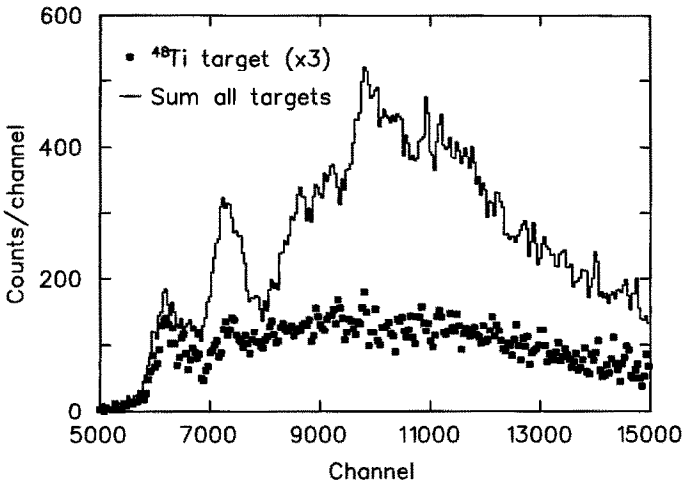

Fig. 2. Proton spectra at zero degrees from Ti metal target, and from metal plus oxide targets. Contributions from ^{16}O(n, p) dominate the sum spectrum above channel 7000 (about 6 MeV excitation in ^{48}Sc).

stack, and counting losses in the wire counters. In practice this correction was made by measuring the relative count rates from a stack of CH_2 targets which could be inserted in place of the targets in the titanium stack.

The zero of the excitation energy scale was established from the location of the ^{1}H(n, p) proton peak at MRS angle of zero degrees. Excitation energies were then determined from focal plane position using the established calibration of the MRS. This calibration could not be checked directly in these measurements since there were no clearly resolved transitions to known states in the ^{48}Ti(n, p)^{48}Sc reaction. From different measurements of the MRS dispersion, however, it is estimated that the energy scale was accurate to ±0.2 MeV at 20 MeV excitation.

3. Results and analysis

Final spectra for the Ti metal target at 0°, 6° and 12° are shown in fig. 3. Comparison of the 0° and 6° spectra shows that the cross sections are peaked at 0° in the region of excitation up to 6 MeV, indicating the presence of $L=0$ transition strength. In order to estimate this quantitatively, data were summed in energy bins 1 MeV in width, and three-point angular distributions were fitted to a sum of DWIA cross sections for $L=0$, 1 and 2. Transitions with $L>2$ are expected to be weak at angles of 0° and 6°, though they could contribute appreciably at 12°. Thus in this analysis the cross section ascribed to $L=2$ transitions may have contributions from higher L-values, although this possibility has little effect on estimates of $L=0$ or $L=1$ strength.

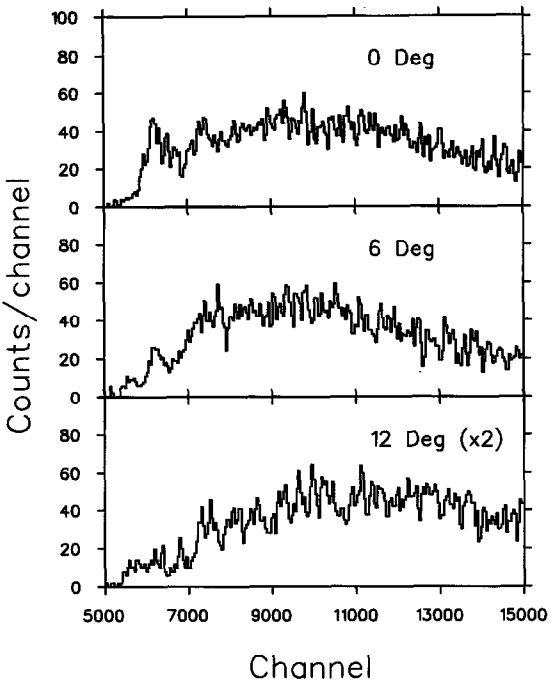

Fig. 3. Proton spectra from the ^{48}Ti metal target at angles of 0°, 6° and 12°. In later analysis the data have been summed in bins of 320 channels width (~1 MeV).

DWIA calculations were carried out using the code DW81 [23]). Microscopic optical potentials were generated using the Franey-Love two-body interaction [24]). For the nuclear structure factor, a number of simple neutron-particle proton-hole configurations were assumed, based on the shell model states expected to be the most important in this mass region. These included the following:

$L=0$: $(f_{7/2}(n)\text{-}f_{7/2}(p^{-1}))$, $(f_{5/2}(n)\text{-}f_{7/2}(p^{-1}))$, $(2p_{3/2}(n)\text{-}2p_{3/2}(p^{-1}))$, $(2p_{1/2}(n)\text{-}2p_{3/2}(p^{-1}))$,

$L=1$: $(g_{9/2}\text{-}f_{7/2})$, $(f_{7/2}\text{-}d_{5/2})$, $(f_{5/2}\text{-}d_{5/2})(2p_{3/2}\text{-}d_{5/2})$, $(2p_{3/2}\text{-}d_{3/2})$, $(2p_{3/2}\text{-}2s_{1/2})$, $(2d_{5/2}\text{-}f_{7/2})$,

$L=2$: $(f_{7/2}\text{-}f_{7/2})$, $(f_{5/2}\text{-}f_{7/2})$, $(2p_{3/2}\text{-}f_{7/2})$, $(2p_{1/2}\text{-}2p_{3/2})$.

In addition, for excitation energies above 12 MeV, calculations for $L=0$ and $L=2$ were carried out for some $2\hbar\omega$ excitations, namely $(g_{9/2}\text{-}d_{5/2})$, $(2p_{3/2}\text{-}1p_{3/2})$, $(f_{7/2}\text{-}1p_{3/2})$. Calculations for a few structure factors were also carried out using empirical

optical potentials derived from analyses of elastic scattering data. The changes in angular distribution shapes for different optical parameters were comparable to those for different structure factors. As a result, it was considered reasonable to base the data analysis on DWIA calculations with only the microscopic potentials.

The shapes of the calculated angular distributions were corrected for the effects of finite target size and MRS acceptance and were then characterized by the ratios $\sigma(\theta°)/\sigma_{max}$ for $\theta = 0°$, 6° and 12°. With this representation angular distributions for $L = 0$ showed little dependence on structure factor, optical potential or excitation energy up to 20 MeV. For $L = 1$ and 2, the ratios showed variations as large as 50% for different structure factors using the microscopic potential. Angular distributions for $L = 0, 1$ and 2 used in the analysis are shown in fig. 4 for $E_x = 3.5$ MeV. The range of shapes obtained for $L = 1$ with different structure factors is also shown.

The data from all targets up to an excitation energy of 6 MeV were analysed to obtain contributions from $L = 0$, 1 and 2 transitions. The analysis was carried out

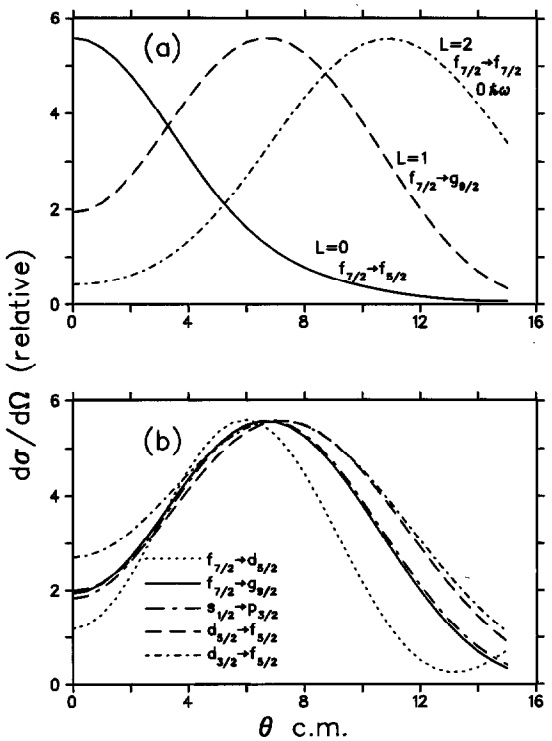

Fig. 4. (a) Standard DWIA shapes used in the multipole analysis. These results are for an excitation energy of 3.5 MeV in ^{48}Sc. (b) Variation in DWIA shapes for $L = 1$ transitions for different structure factors. Curves are arbitrarily normalized to the same peak cross section. The distributions for $(f_{5/2}(n)$-$d_{3/2}(p^{-1}))$, $(g_{9/2}(n)$-$f_{7/2}(p^{-1}))$ and $(2d_{5/2}(n)$-$f_{7/2}(p^{-1}))$ are referred to as flat, standard and peaked, respectively.

using $L=1$ shapes corresponding to the most strongly peaked distributions the flattest distributions and "average" shape corresponding to the structure factors expected to be most important in a simple shell model description of ^{48}Ti.

The results of this analysis are shown in fig. 5, where the measured cross section at 0° is compared with our estimate of $L=0$ cross section at 0° for excitation energies up to 6 MeV in ^{48}Sc. It is clear that there is considerable $L=0$ strength in this region, and that the estimate of strength is not very sensitive to variations in the shape of the $L=1$ angular distribution up to 4.5 MeV. At 5.5 MeV and higher excitation, contributions to the cross section from the ^{16}O(n, p) reaction result in increased sensitivity to the shape of the $L=1$ distribution, and greater uncertainty in the estimate of the $L=0$ cross section.

A similar analysis extending to higher excitation energies was carried out using data from the Ti metal target only. In this case DWIA calculations were carried out for several excitation energies of up to 20 MeV, to obtain the energy dependence of the angular distributions, and these were used to fit the data. For $L=1$, a structure factor $(g_{9/2}(n)\text{-}f_{7/2}(p^{-1}))$ was assumed. For $L=2$ the structure factor was $(f_{5/2}\text{-}f_{7/2})0\hbar\omega$ up to 8 MeV and an average of $(g_{9/2}\text{-}d_{5/2})$ and $(f_{7/2}\text{-}1p_{3/2})2\hbar\omega$ above 12 MeV, with a smooth interpolation between 8 and 12 MeV.

Results of this analysis are shown in fig. 6. At excitation energies above about 15 MeV, the estimate of $L=0$ strength depends sensitively on the shape of the $L=1$ angular distributions. This result reflects the fact that in this region of excitation the experimental angular distributions are nearly flat so that any estimate of the

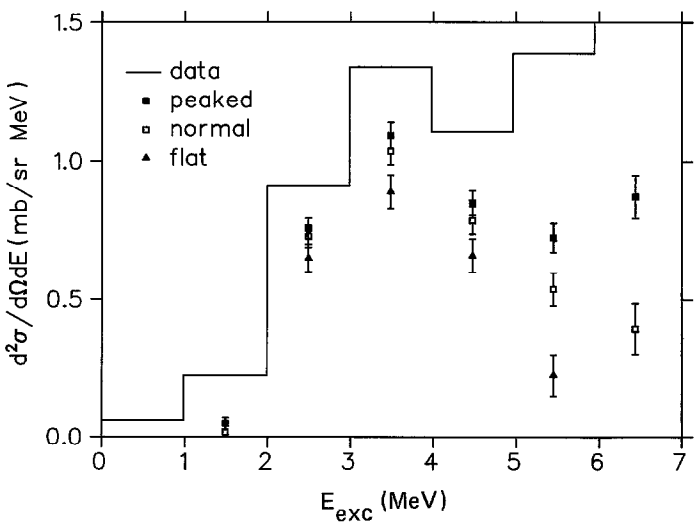

Fig. 5. Comparison of the measured 0° cross section for the sum of the metal plus oxide targets, shown by the solid line, with the extracted $L=0$ contribution. Results are shown for three different choices of structure factors for $L=1$ DWIA calculations, as noted in the caption to fig. 4.

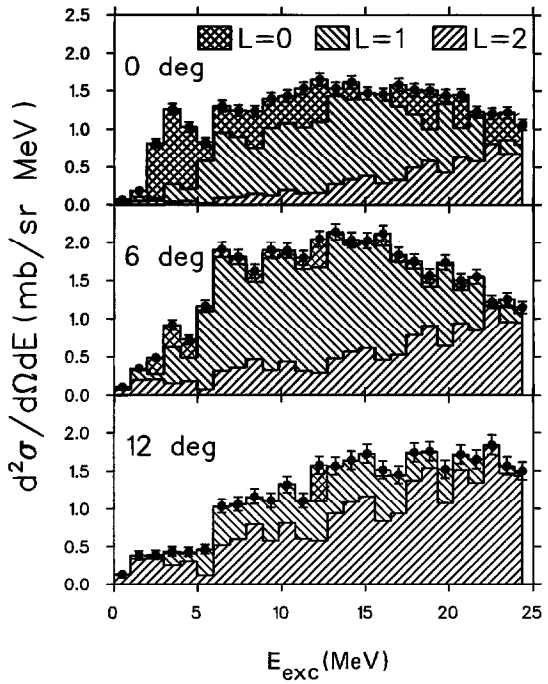

Fig. 6. Multipole decomposition of cross sections at 0°, 6°, 12° using "standard" DWIA shapes. See fig. 4.

forward-peaked $L=0$ strength is strongly affected by the calculated zero degree reaction for $L=1$, and to a lesser extent for $L=2$, transitions. It is clear, however, that this analysis finds $L=0$ transition strength in the region between 6 and 12 MeV excitation which though dependent on the structure factors assumed for $L=1$ and 2 is non-zero even for the flattest $L=1$ distribution. In this region, a lower limit to the $L=0$ strength would be that obtained with structure factors which yield no contribution for $L=0$ at energies above 15 MeV. Larger-scale structure calculations to provide more realisic structure factors, and their variation with excitation energy, would be required for any more quantitative estimate of $L=0$ strength at higher excitations.

These results show that $L=1$ strength is distributed more or less uniformly between 6 and 20 MeV excitation and presumably defines the region of the spin-dipole giant resonance. The total cross section at 6° for $L=1$ transitions is 23 mb/sr, with an estimated uncertainty of about 30% arising from the use of different $L=1$ structure factors.

Similar results are found for $L=2$ (actually $L\geqslant 2$) strength. Only a small amount of strength is observed below about 6 MeV excitation. At higher energies, the strength per unit energy range increases linearly, within the experimental uncertainties, up to the highest energy observed, about 24 MeV. Once again the strength distribution

is not sensitive to the choice of transition amplitudes, although the total strength is uncertain by nearly a factor of two.

3.1. MODEL COMPARISONS

For comparison with model calculations of the GT strength distribution, the measured cross sections have been expressed in terms of GT strength, following a procedure similar to that of ref. [3]). A correction for the dependence of the cross section on reaction Q-value and momentum transfer was made by multiplying the measured cross section by the ratio $\sigma_{DW}(Q=q=0)/\sigma_{DW}(Q, q)$, where the values of Q and q in the denominator are appropriate for the experimental cross section. The value $\hat{\sigma}=\sigma(Q=q=0)/B_{GT}=5.3$ was then used to convert reaction cross sections to GT strength.

It is noted [3]) that experimental values of $\hat{\sigma}$ may exceed the results of DWIA calculations by as much as 50%. From the results quoted, however it is seen that such large deviations occur only for odd-A target nuclei, and particularly for transitions between isobaric analog states involving both GT and Fermi components. For even-A targets of mass $A \lesssim 60$, the empirical differences are about $\pm 10\%$. This is also the magnitude of differences found between DWIA calculations with different transition amplitudes for a given pair of states.

The total GT strength up to 15 MeV obtained using the "standard" shape for $L=1$ transitions is $\sum B_{GT}=1.42\pm 0.2$. The quoted uncertainty arises from statistical uncertainties in the data only, and does not include any possible systematic error arising from uncertainties in the value of $\hat{\sigma}$. A similar analysis using the "flat" $L=1$ shape yields a value $\sum B_{GT}=1.19\pm 0.2$. This "flat" shape gives the largest possible contribution to the $L=1$ cross section at zero degrees, within the $1\hbar\omega$ model space assumed in the DWIA calculations. Thus, within this model space, the value $\sum B_{GT}=1.19\pm 0.2$ is a lower limit to our estimate of GT strength in this region.

Fig. 6 indicates some $L=0$ contribution to the cross section at excitation energies greater than 15 MeV, using the "standard" $L=1$ shape but the significance of this result is questionable. If the "flat" shape is used, the analysis yields the unphysical result of negative values for the $L=0$ cross section in some regions of the spectrum.

Calculations of the GT strength distribution for ^{48}Ti(n, p) have been carried out by Tsuboi *et al.* [14]), by Brown [19]) and by Engel [26]). The first two involve shell model calculations in a model space $(f_{7/2})^{8-n}(f_{5/2}p_{3/2}p_{1/2})^n$ with $n=0, 1, 2$. The third is a quasiparticle RPA calculation, including particle-particle interactions in the final state. The measured strength distribution for the "standard" $L=1$ shape is shown in fig. 7a along with results of the two shell model calculations. Both models predict strength at higher excitations, to 15 MeV in ref. [14]), and 26 MeV in ref. [19]), but it is too small to display on fig. 7. The results of both calculations have been renormalized by a factor 0.6, which has been found to be appropriate for comparisons of theory and experiment for (sd) shell nuclei [27]). The total strength predicted by Tsuboi *et*

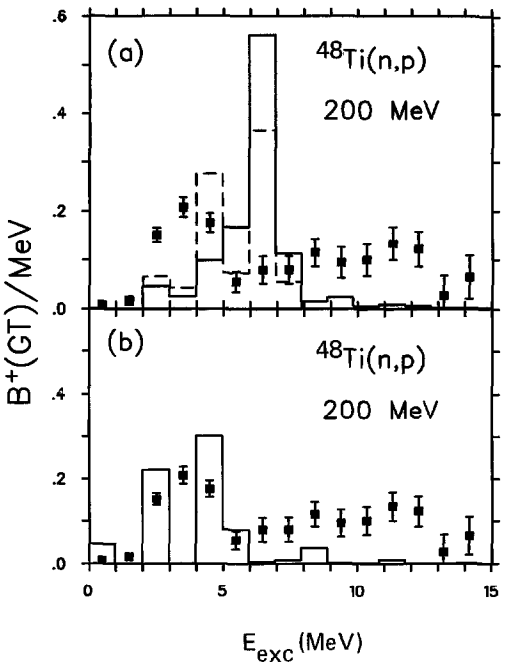

Fig. 7. (a) Comparison of measured GT strength distribution with shell model calculations dashed line - ref. [14]), solid line - ref. [19]). Experimental uncertainties are statistical only. Systematic uncertainties arising from the multipole decomposition of the spectra are discussed in the text. (b) Comparison of measured GT strength distribution with QRPA calculations from ref. [26]).

al. is $B_{GT} = 0.88$, and by Brown $B_{GT} = 1.04$, in both cases in reasonable agreement with the data. It is seen, however, that both calculations predict a concentration of strength near 6 MeV excitation, in poor agreement with the data, and fail to account for the strength at excitations above 7 MeV.

The QRPA calculation, renormalized by the same factor of 0.6, predicts a total GT strength of 0.71 units. It should be noted that this calculation introduces two adjustable parameters. The first, the strength of the particle-particle interaction, is set to a value of -380 MeV $\cdot$ fm^3, a value close to that used in double beta decay calculations for heavier nuclei in ref. [28]). The second is the location of the zero of excitation energy in ^{48}Sc; here again we have used the same procedure as in ref. [28]), setting the energy of the lowest strong, transition equal to that of the first 1^+ state at 2.52 MeV in ^{48}Sc. These are discussed in the context of (fp) shell nuclei in ref. [29]). The resulting strength distribution, shown in fig. 7b reproduces the low-lying part of the spectrum, but shows little strength above 6 MeV. It is also seen that if the energy of the lowest 1^+ state is set equal to 2.52 MeV, then the QRPA results are very similar to the shell model calculations.

The most reliable experimental result obtained from this measurement is the total strength of 0.54 units distributed between 2–5 MeV in excitation energy. As can be

seen in fig. 7, this result is in qualitative disagreement with the present shell model calculations which put little strength in this region but instead predict a concentration in the 4–7 MeV range. This qualitative result is important to take into account for any new calculations of the double beta decay. Several calculations are under way [25,30]), and the preliminary results from ref. [25]) indicate that the strength distribution for these ^{48}Ti to ^{48}Sc matrix elements is indeed very sensitive to the interaction used and to the model-space truncations.

3.2. LIFETIME FOR DOUBLE BETA DECAY

Although there has been considerable interest in the double beta decay of ^{48}Ca, as indicated by the many theoretical studies reported, there has been only a single experimental search for the process [31]). In addition, a search for the single beta decay of ^{48}Ca, which is energetically allowed but highly forbidden by a large change in spin, has been reported [32]). Neither decay was observed, but lower limits were established: $t_{1/2} > 6 \times 10^{18}$ y for single and $> 3.6 \times 10^{19}$ y for double beta decay. The experimental limit on the double beta decay half-life, along with several theoretical limits, are listed in table 1. It is seen that some of the calculations are consistent with the experimental result, but that different calculations disagree with one another by a factor of up to 10, as a result of differing assumptions and approximations and correction factors introduced into each of the calculations.

The results of the present measurement, taken along with results from a study of the ^{48}Ca(p, n) reaction [33]) might be used to estimate the expected half-life, although this would be subject to very large uncertainties. Although the GT strength distributions in ^{48}Ca(p, n) and ^{48}Ti(n, p) provide a measure of the magnitude of the matrix elements of interest in the calculation of $M_{2\nu}$ [eq. (1)], the sign of the matrix elements is not determined. The following analysis will indicate the sort of comparison that can be made.

TABLE 1

Estimates of double beta lifetime of ^{48}Ca

	$T_{1/2}$ [10^{19} y]
Experiment [31])	>3.6
Brown [19])	9.0
Tsuboi *et al.* [14])	1.7 [a])
Haxton and Stephenson [12])	7.5 [a])
Engel [26])	0.9

[a]) Published results for refs. [12,14]) have been renormalized by a factor of 0.36 corresponding to a renormalization of individual matrix elements by a factor of $\sqrt{0.6}$.

Studies of the ^{48}Ca(p, n) [ref. [33])], ^{46}Ca(^{3}He, p) [ref. [34])] and ^{48}Ti(t, ^{3}He) [ref. [35])] reactions have identified many 1^+ states in ^{48}Sc at excitation energies up to 6 MeV. With the relatively poor energy resolution in the present results, it is not possible to obtain an unambiguous measurement of cross sections for transitions to known 1^+ states. We have, however, carried out an analysis of the zero degree data at low excitation on the assumption that the lowest 1^+ states populated in the present measurements are the same as those observed in ^{48}Ca(p, n)^{48}Sc. This latter measurement identifies GT transitions to the lowest 1^+ state at 2.52 MeV, plus states at 3.09, 3.60 and 5.38 MeV. We have fitted the zero degree spectrum assuming peaks at these energies, and at the location of the strong ^{16}O(n, p) transitions. In addition we assume a background which increases quadratically to represent the effect of increasing contributions from transitions with $L > 0$ as indicated in fig. 6. Each peak has a fixed gaussian shape with FWHM of 1.3 MeV. This procedure provides a poor fit to the data, but when the assumption of a peak at 5.38 MeV is relaxed and the program is allowed to search on the location of that peak, an excellent fit is obtained with a peak at an energy of 4.6 ± 0.1 MeV A 1^+ state has been identified at $E_x =$ 4.69 MeV in the ^{46}Ca^{3}(He, p) measurements [34]), and this result confirms theoretical predictions that the relative population of 1^+ states may be quite different in (p, n) and (n, p) reactions [14,19]).

The resulting fit is shown in fig. 8. The same result, with larger statistical uncertainties, is obtained if the spectrum from the Ti metal target alone is fitted. If, in addition to peaks at 2.52, 3.09, 3.60 and 4.6 MeV, a peak fixed at 5.38 MeV is included in

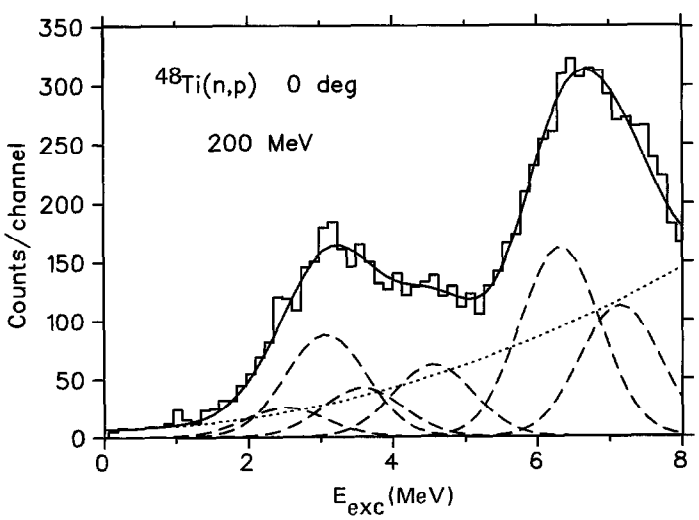

Fig. 8. Decomposition of 0° cross section at low excitation assuming transitions to discrete states in ^{48}Sc. The peaks above 6 MeV arise from ^{16}O(n, p). The solid curve through the data is the sum of the peaks shown plus a quadratically increasing background up to 8 MeV.

the analysis, the last peak has zero amplitude, within statistical uncertainties. The cross sections for the transitions to these states along with corresponding GT strength are listed in table 2.

We note that the assignment of strength to states at 3.09 and 3.60 MeV assumes that the same state are excited in both (p, n) and (n, p) reactions. We have observed however that a state at 5.38 MeV is excited only in (p, n), while at a state of 4.6 MeV is excited only in (n, p). In fact, calculations [19,25]) indicate that there should be five to seven 1^+ states in the 2-5 MeV energy range, and their population is in general quite different in the (p, n) and (n, p) reactions. A recent (t, ^{3}He) measurement [35]) indicates probable 1^+ states relatively strongly excited at 2.989, 3.064 and 3.719 MeV. With the resolution of about 1.3 MeV in the present measurements we are unable to conclude whether the first two states are involved in the transition which we identify at 3.09 MeV or the state at 3.719 MeV in the transition at 3.60 MeV.

In spite of these uncertainties, the data for the region of low excitation may be used to provide a rough estimate of the double beta decay lifetime, based on the following assumptions: (i) the states at 2.52, 3.09 and 3.60 MeV are populated in both (p, n) and (n, p) reactions; (ii) the 4.6 [5.38] MeV state is populated in the (n, p)[(p, n)] but not the other reaction; (iii) all individual matrix elements have the same sign. With these assumptions the value of $M_{2\nu}$ [eq. (1)] is 0.11 MeV^{-1} for states up to 5.38 MeV. The phase space factor $f_{2\nu}$ for ^{48}Ca decay may be obtained from the calculated lifetime [14]) and has the value 7.6×10^{-18} y^{-1} MeV^2, yielding a half-life of $t_{1/2}=7.5\times10^{18}$ y, which is significantly shorter than the limit reported in ref. [31]). It must be recognized however that observed strength at higher excitation is not considered in this estimate. In the shell model calculations [14,19]), contributions to the matrix element from states above 6 MeV are predicted to have about half the magnitude of low-lying contributions, but with opposite sign. Thus the matrix element could well be reduced by a factor of two, resulting in a fourfold increase in the estimate of the lifetime.

TABLE 2

Zero-degree cross sections and GT strength from peak fitting at low excitation

Peak E_x [MeV]	$\sigma(0°)_{c.m.}$ [mb/sr]	B (GT) [b])
2.52	0.31 ± 0.03 [a])	0.07
3.09	1.05 ± 0.03	0.22
3.60	0.50 ± 0.03	0.11
4.6	0.74 ± 0.04	0.16

[a]) Statistical uncertainty only. Systematic uncertainties are estimated to be approximately 10%.

[b]) Obtained using the calculated value $\hat{\sigma}=5.3$. Systematic uncertainties in this value are discussed in the text.

4. Conclusions

Measurements of the ^{48}Ti(n, p)^{48}Sc reaction have been made at angles of 0°, 6° and 12° at an incident energy of 200 MeV with experimental energy resolution of about 1.3 MeV. The resultant cross sections have been compared with DWIA calculations for angular momentum transfers of $L = 0$, 1 and 2, in order to estimate the cross sections for each angular momentum as a function of excitation energy. The $L = 0$ cross section, which measures GT strength, is most prominent at low excitation, which significant contributions extending to about 15 MeV. The experimental GT strength distribution has been compared with results of model calculations using two different shell models, and with results of a QRPA calculation. The shell model calculations predict a concentration of GT strength near 6 MeV excitation appreciably above the observed maximum between 3 and 4 MeV. The QRPA result fits the observed distribution of low-lying strength somewhat better, but the quality of the fit depends on the zero of energy chosen in the calculation. None of the calculations account for the strength observed between 7 and 15 MeV excitation.

The GT strength at these higher excitations is expected to be important in determining the ^{48}Ca double beta decay lifetime, since much of the strength in the GT giant resonance observed in ^{48}Ca(p, n) is found in this region. The failure of the model calculations to account for the strength in this region means that model estimates of the ^{48}Ca double beta decay lifetime are subject to large uncertainties.

The authors would like to thank N. Auerbach and D. Wilkinson for discussions and helpful suggestions. We also acknowledge the cooperation and assistance of the TRIUMF technical staff in carrying out this experiment.

This work was supported by the National Research Council and the Natural Sciences and Engineering Research Council of Canada.

References

1) T.N. Taddeucci *et al.*, Phys. Rev. **C25** (1982) 1094
2) C.D. Goodman *et al.*, Phys. Rev. Lett. **44** (1980) 1755
3) T.N. Taddeucci *et al.*, Nucl. Phys. **A469** (1987) 125
4) K.P. Jackson *et al.*, Phys. Lett. **B201** (1988) 25
5) F. Osterfeld, D. Cha and J. Speth, Phys. Rev. **C31** (1985) 371
6) S. Yen *et al.*, Phys. Lett. **B206** (1988) 597
7) M.C. Vetterli *et al.*, Phys. Rev. Lett. **59** (1987) 439
8) D. Krofchek *et al.*, Phys. Lett. **B189** (1987) 299
9) P. Vogel, M. Ericson and J.D. Vergados, Phys. Lett. **B212** (1988) 259
10) T. Kirsten *et al.*, in Proc. Int. Symp. on nuclear beta decays and neutrinos, ed. T. Kotani, H. Ejiri and E. Takasugi (World Scientific, Singapore, 1986) p. 81
11) S.R. Elliott, A.A. Hahn and M.K. Moe, Phys. Rev. Lett. **59** (1987) 1649
12) W.C. Haxton and G.J. Stephenson Jr., Prog. Part. Nucl. Phys. **12** (1984) 409
13) D.O. Caldwell *et al.*, Phys. Rev. **D33** (1986) 2737
14) T. Tsuboi, K. Muto and H. Horie, Phys. Lett. **B143** (1984) 293
15) J.D. Vergados, Phys. Reports **133** (1986) 1

16) H.V. Klapdor and K. Grotz, Phys. Lett. **B142** (1984) 323
17) P. Vogel and M.R. Zirnbauer, Phys. Rev. Lett. **57** (1986) 3148
18) O. Civitarese, A. Faessler and T. Tomoda, Phys. Lett. **B194** (1987) 11
19) B.A. Brown, in Nuclear shell models, ed. M. Vallieres and B.H. Wildenthal (World Scientific, Singapore, 1985) p. 42
20) T. Tomoda and A. Faessler, Phys. Lett. **B199** (1987) 475
21) R. Helmer, Can. J. Phys. **65** (1987) 588
22) R. Henderson *et al.*, Nucl. Instr. Meth. **A257** (1987) 97
23) R. Schaeffer and J. Raynal, Computer Code DWBA70, unpublished, Arizona State University (1984); J.R. Comfort, Computer Code DW81 (extended version of DWBA70), Arizona State University, 1984.
24) M.A. Franey and G. Love, Phys. Rev. **C31** (1985) 488
25) L. Zhao and B.A. Brown, unpublished
26) J. Engel, unpublished
27) B.A. Brown and B.H. Wildenthal, Phys. Rev. **C28** (1983) 2397
28) J. Engel, P. Vogel and M.R. Zirnbauer, Phys. Rev. **C37** (1988) 731
29) J. Engel, P. Vogel, O. Civitarese and M.R. Zirnbauer, Phys. Lett. **B208** (1988) 187
30) T. Shinozuka *et al.*, in Abstracts of Invited and Contributed Papers, XXII Yamada Conf. on nuclear weak processes and nuclear structure, Osaka, 1989 p. 108
31) R.K. Bardin, P.J. Gollon, J.D. Ullman and C.S. Wu, Nucl. Phys. **A158** (1970) 337
32) D.E. Alburger and J.B. Cumming, Phys. Rev. **C32** (1985) 1358
33) B. Anderson *et al.*, Phys. Rev. **C31** (1985) 1161
34) D.G. Fleming, O. Nathan, H.B. Jensen and O. Hansen, Phys. Rev. **C5** (1972) 1365
35) F. Ajzenberg-Selove, Ronald E. Brown, E.R. Flynn and J.W. Sunier, Phys. Rev. **C32** (1985) 756